2021 43rd Annual International Conference of the
IEEE Engineering in Medicine & Biology Society (EMBC)
Oct 31 - Nov 4, 2021. Virtual Conference

An *in silico* trials platform for the evaluation of effect of the arterial anatomy configuration on stent implantation*

Georgia S. Karanasiou, Panagiota I. Tsompou, Nikolaos Tachos, Gianna E. Karanasiou, Antonis Sakellarios, Savvas Kyriakidis, Luca Antonini, Giancarlo Pennati, Lorenza Petrini, Frank Gijsen, Farhad Rikhtegar Nezami, Rami Tzafriri, Martin Fawdry, Dimitrios I. Fotiadis, *Fellow, IEEE*

***Abstract*—The introduction of Bioresorbable Vascular Scaffolds (BVS) has revolutionized the treatment of atherosclerosis. InSilc is an *in silico* clinical trial (ISCT) platform in a Cloud-based environment used for the design, development and evaluation of BVS. Advanced multi-disciplinary and multiscale models are integrated in the platform towards predicting the short/acute and medium/long term scaffold performance. In this study, InSilc platform is employed in a use case scenario and demonstrates how the whole *in silico* pipeline allows the interpretation of the effect of the arterial anatomy configuration on stent implantation.**

I. Introduction

The medical devices market reached approximately 457 billion euro in 2019, achieving a compound annual growth rate (CAGR) of 4.4%, since 2015, and is expected to reach 603.5 billion euro by 2023 [1]. To be released to the market, any biomedical device needs to demonstrate its reliability, safety and efficacy on the defined target population for the selected clinical application. This is a time consuming and costly process requiring the creation, analysis and delivery of manufacturing, pre-clinical (from animals) and clinical evidence (from humans). Despite the continual improvement of biomedical device pipeline methodologies, there are still instances where products demonstrate very good preclinical performance, but are non-efficacious or present severe complications and side effects during clinical trials. This can be attributed to the complexity of the human anatomy and physiology and the differences observed between the enrolled patient populations. Depending on the phase of the medical device failure, the implications in terms of time, cost but most importantly ethical considerations, differ. Additionally, there are no indicators suggesting the cause of safety or efficacy concerns for identifying the required improvements. This challenge could be met by the introduction of the promising approach of *in silico* modelling that involves the combination of biological data and biomedical knowledge and their integration in computer-based representations. In fact, this fast-emerging technology can be considered as the third pillar for partially refining, replacing and reducing the *in vitro, in vivo* and real clinical trials and answer to several "What if" scenarios. *In silico* medicine targets the prevention and treatment of diseases, considering patient- and/or device specific parameters of interest, which are hard or even impossible to be estimated. In parallel, *in silic*o clinical trials (ISCT) are being created for delivering personalised computer simulations to be used in the design, development or even regulatory evaluation of a medical device and/ or intervention.

II. *From Computational Modeling to In Silico Clinical Trials*

A. The Concept

ISCT involves the development of computational models and their utilisation to a patient in order to simulate the disease and the medical device implantation process. These models can provide predictions of the outcome and can be used in parallel with an existing clinical trial. Then in order to evaluate the predictive accuracy of the computational models, the *in silico* results are compared with the real clinical trials observations. As soon as this process is applied to a sufficient number of patients, these data can be accompanied with additional clinical information to create the "virtual populations". The latter are then used to perform *in silico*

* Research supported by the InSilc project that has received funding from the European Union's Horizon 2020 research and innovation program under grant agreement No 777119.

G.S. Karanasiou, N. S. Tachos, G. E. Karanasiou, A. Sakellarios, S. Kyriakidis, is with the Department of Biomedical Research, Institute of Molecular Biology and Biotechnology, FORTH, GR 45110, Ioannina, Greece, (email: g.karanasiou@gmail.com, ntachos@gmail.com).

P. I. Tsompou is with Unit of Medical Technology and Intelligent Information Systems, Dept. of Materials Science and Engineering, University of Ioannina). GR 45110, Greece (emails: panagiotatsompou@gmail.com,).

L. Antonini and G. Pennati are with LaBS, Dept. of Chemistry, Materials and Chemical Engineering "Giulio Natta", Politecnico di Milano, Milan, Italy (email: luca.antonini@polimi.it, giancarlo.pennati@polimi.it).

L. Petrini is with LaBS, Dept. Civil and Environmental Engineering, Politecnico di Milano, Milan, Italy (email: lorenza.petrini@polimi.it).

F. Gijsen is with the Dept. of Cardiology, Erasmus MC, University Medical Center Rotterdam, Rotterdam, the Netherlands (email: f.gijsen@erasmusmc.nl).

F. R. Nezami and R. Tzafriri are with Harvard-MIT Biomedical Engineering Center, Institute for Medical Engineering and Science Massacusetts Institute of Technology, Cambridge, MA 02139. USA (email: farhadr@mit.edu, rtzafriri@cbset.org)

T. Vaghan is with the Biomechanics Research Centre, School of Engineering, College of Science and Engineering, National University of Ireland Galway, Ireland (email: ted.vaughan@nuigalway.ie).

M. Fawdry is with the Corporate Research and Global Technology and Services groups, Boston Scientific Limited, Galway, Ireland, H91 Y868 (email: fawdrym@bsci.com)

D.I. Fotiadis is with the Department of Biomedical Research, Institute of Molecular Biology and Biotechnology, FORTH, Ioannina, Greece and the Dept. of Materials Science and Engineering, Unit of Medical Technology and Intelligent Information Systems, University of Ioannina, GR 45110, Ioannina, Greece (phone: +302651009006, fax: +302651007092, e-mail: fotiadis@cc.uoi.gr).

experiments towards the evaluation of an existing or new biomedical device.

B. InSilc approach

InSilc is a cloud-based *in silico* platform targeting the design, development and evaluation of Bioabsorbable Vascular Stent (BVS) towards their application in *in silico* trials [4]. The platform integrates advanced multi-scale models considering different biological processes and mechanisms, achieving the simulation of BVS mechanical, deployment and degradation, fluid dynamics and drug-delivery performance in the short/acute- and medium/long term.

C. What if scenarios

InSilc is a platform designed for BVS, however, its applicability can be extended to any coronary stent, including the Drug-eluting stents (DES) and the Bare-Metal Stents (BMS). Therefore, after an extensive analysis and evaluation of the existing studies and considering the needs of the Stent Industry, we have designed the following scenarios (SC) of use: Comparison of existing stents in the same virtual population (***Scenario I***), Comparison of stent performance in different anatomy configurations (***Scenario II***), Comparison of stent performance in different clinical procedures (***Scenario III***) and, Design of entirely new stents (***Scenario IV***). In this study, we will demonstrate how Scenario II can be applied for comparing the performance of the Synergy stent, a Platinum-Chromium alloy stent by Boston Scientific [2], in two different arterial configurations. The demonstration of Scenario II is realized through the integration and communication of the following Modules/Tools: (i) 3D Reconstruction and Plaque Characterization Tool, (ii) Deployment Module, (iii) Fluid-dynamics Module and, (iv) Drug-delivery Module.

D. In Silico Pipeline

3D Reconstruction and Plaque Characterization Tool. The first tool used in scenario II is the 3D Reconstruction and Plaque Characterization Tool. This tool includes a methodology that applies advanced image processing algorithms for the reconstruction of a patient specific arterial wall. This is accomplished through the utilization of imaging information from: OCT and the fusion with angiography. In this scenario, we used data from two patients (patient A, patient B) participating in a prospective study with 100 patients, taking place in the University Hospital of Ioannina (UOI), Greece and in the Erasmus Medical Center (ERASMUS), Netherlands. In more detail: (i) from both patients, OCT and angiography data were used, (ii) patient A was a 47 years old female and patient B was a 45 years old female, (iii) the Synergy stent was implanted in the mid-vessel left anterior descending (LAD) coronary artery in both patients. To create the 3D arterial walls and the underlying plaques, the methodology as defined in [3], has been followed. In brief, initially the registration of the angiographic views with the OCT pullback and the selection of R-peak OCT frames were performed. Then, the lumen and adventitia borders detection on the OCT frames was achieved. From the angiographic views, an automatic extraction of 2D centerlines was accomplished followed by the fusion of 2D centerlines towards the creation of the final 3D centerline. The OCT segmented R-peak frames were perpendicularly positioned in the 3D centerline and by taking as landmarks the annotated branches of the OCT frames for the absolute orientation of the 3D model, the final 3D arterial model was created (Fig. 1).

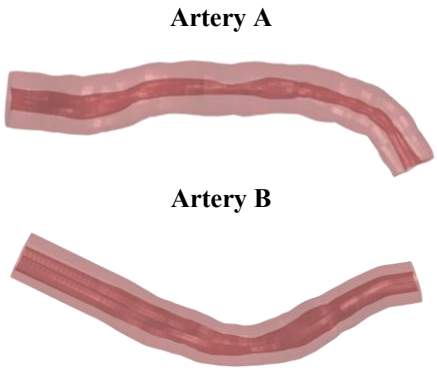

Figure 1. 3D reconstructed arteries from OCT and angiography: (i) Artery A from patient A (from UOI), (ii) Artery B from patient B (from ERASMUS).

Deployment Module. The Deployment Module allows the creation of stent deployment simulations within realistic imaged-based stenotic coronary arterial models created by the 3D Reconstruction and Plaque Characterization Tool. These simulations involve mutual interaction between the finite element model of the coronary artery, the delivery system (i.e. stent and balloon) and additional balloons used for any possible angioplasty, post-dilation or other procedures. The artery was discretized with reduced-integration hexahedral elements (C3D8R) and described mechanically by subdividing it into three layers, namely adventitia, media and diseased-intima, and by identifying areas of calcific plaque and lipid pools on the basis of data deriving from the 3D Reconstruction and Plaque Characterization Tool. The stent, also meshed with C3D8R elements, is mechanically described through a bilinear elastic-plastic material model. As far as the balloons are concerned, they were modelled with a simplified design (membrane elements, M3D4) able to faithfully replicate the physical behavior of the real device in terms of pressure-diameter relationship. For this scenario, it was decided to computationally imitate the real clinical procedure of patient A, i.e. an angioplasty followed by implantation of the Synergy stent. The simulations were organized in successive steps: in the first step, the angioplasty balloon and the delivery system were placed inside the vessel lumen; then the pre-dilatation of the artery was simulated by inflating and deflating the angioplasty balloon and finally the deployment of the stent took place. Outputs of Deployment module allow to verify effects of the stenting procedure immediately after the deployment. In terms of clinical endpoints, it is possible to evaluate the lumen gain and eventually malappositions. In the presented scenario, no malappositions were detected and a lumen gain of 105% and 30% were reached in case A and B, respectively (Fig. 2). Moreover, the results of simulations allow a refinement of the data commonly available in acute conditions: from the map of maximum stresses in the stent struts and maximum strain in the coronary tissue (Fig. 2), possible risks of arterial wall or device damage can be evaluated. In particular, the simulations show the effectiveness of Synergy stent in reopening the lumen in both

cases without risk of stent damage. However, Artery A, where a more severe and localized stenosis was present, is subjected to higher and more distributed deformation that could lead to restenosis.

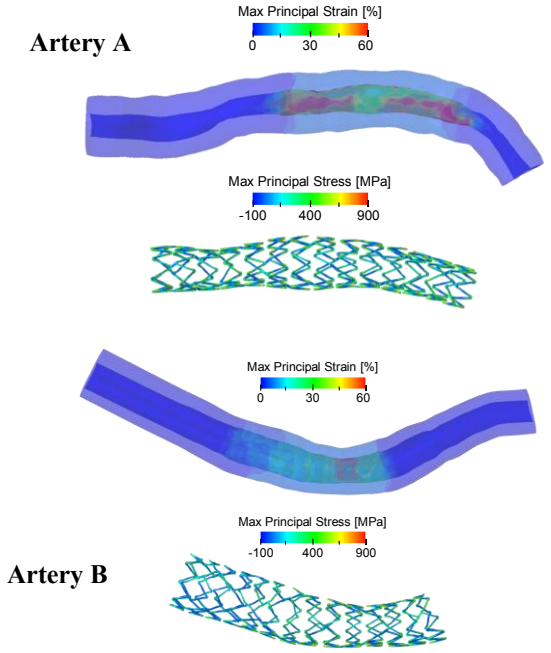

Figure 2. Comparison between the final configurations obtained at the end of the deployment simulations: (i) Artery A from patient A, (ii) Artery B from patient B.

Fluid Dynamics Module. The post-deployment geometries, as computed by the Deployment Module, were used in the Fluid Dynamics Module to simulate blood flow through the stented vessels. Time-dependent Computational Fluid Dynamics (CFD) simulations were performed for the two post-deployment geometries from scenario II using ICEM (Ansys ICEM, release 20.1) for meshing and Fluent (Ansys Fluent, release 20.1) for CFD. In the simulations, blood was assumed as an incompressible, homogeneous, Carreau fluid. For the boundary conditions a generic transient flow profile for the LAD [4] is used at the inlet, with the mean flow scaled to the inlet diameter of the specific geometry following the flow-diameter relation described in [5]. At the outflow an 'outflow' boundary condition was used [6]. The CFD simulation was performed over two heart cycles.

Post-processing of the simulation results was done in MATLAB (R2018a, Mathworks Inc). Time Averaged Wall Shear Stress (TAWSS) was computed by averaging the computed wall shear stresses over the last heart cycle. The Oscillatory Shear Index (OSI) was computed as the ratio between back- and forward going shear stress. The vessels were folded open in the longitudinal direction to generate 2D maps of TAWSS and OSI using VMTK (The Vascular Modeling Toolkit website, www.vmtk.org). TAWSS and OSI for the two post-deployment patient geometries are shown in for patient A in Fig. 3 and for patient B in Fig. 4. The figure shows the TAWSS on the vessel wall of the 3D geometry as well as 2D maps of the folded-open vessel wall for both TAWSS and OSI in the segment with the scaffold. Histograms of TAWSS and OSI are shown to indicate the WSS distribution over the vessel wall.

A fairly uniform TAWSS distribution was found for patient A, with the majority of the TAWSS in the physiological range. In patient B, we clearly identify local narrowing of the vessel, leading to locally increased TAWSS values, but overall TAWSS seems to be lower. For both patients, OSI is very low. The histograms allow us to further quantify these results: when using 0.5 Pa as a threshold for adverse TAWSS [7], we observe that for patient A 36% of the area is exposed to low TAWSS, while for patient B 54% of the stented area is exposed to low TAWSS. This implies that the hemodynamic environment for patient A is more favorable than for patient B.

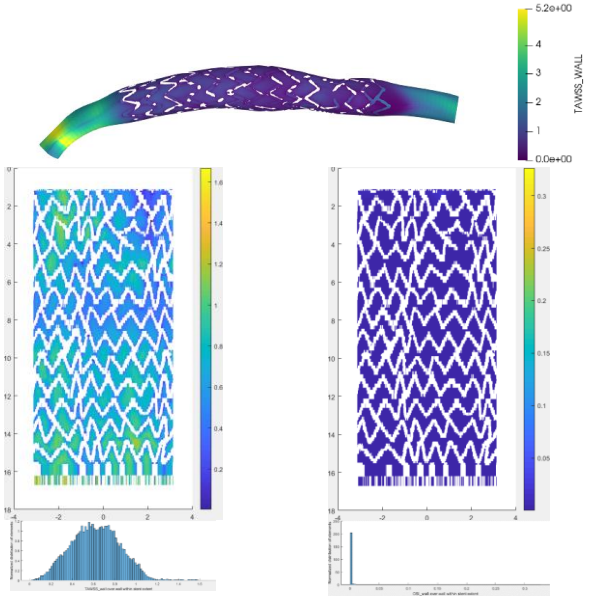

Figure 3: 3D TAWSS (up) and 2D maps of TAWSS (left) and OSI (right) for patient A. The histograms corresponding to the 3D maps are shown in the bottom row.

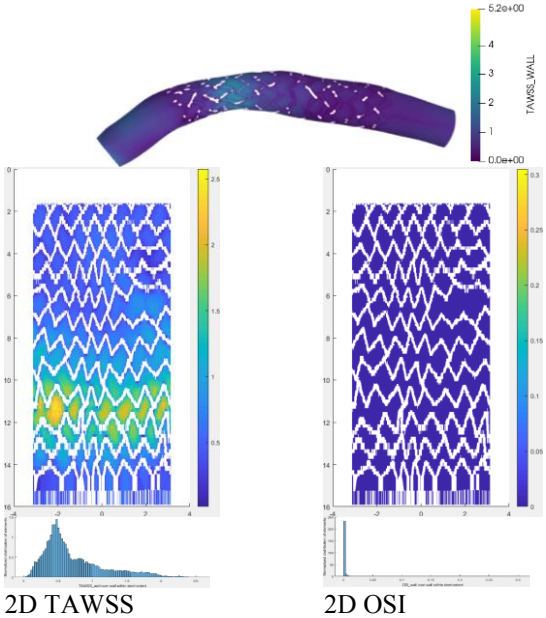

Figure 4: 3D TAWSS (up) and 2D maps of TAWSS (left) and OSI (right) for patient B. The histograms corresponding to the 3D maps are shown in the bottom row.

Drug-delivery Module. The Drug Delivery Module allows the simulation of release kinetics from the stent coating and prediction of the spatiotemporal distribution of drug in the patient-specific arterial geometry provided by the deployment module. Everolimus drug release from the poly(lactic-co-glycolic acid) (PLGA) coating of the Synergy stent is modeled based on an analytical solution of dispersed drug dissolution and diffusion equations in a degrading polymer, that correctly accounts for the burst and sustained phases of *in vivo* drug release in animal data (Fig. 5, [8]).

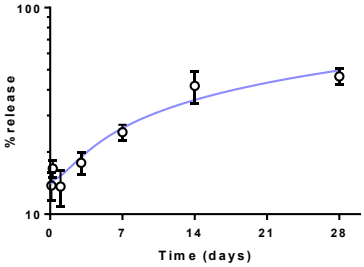

Figure 5: Synergy release kinetics, modeling (lines) versus *in vivo* data (symbols) [8]

Drug release applied as a surface flux at coated abluminal strut interfaces drives a computational model of tissue distribution that accounts for extracellular convection, diffusion and binding as well as high affinity intracellular binding. The results of Deployment Module for the deformed artery and the deployed device were received as 3D triangulated surface files (STL format), and, after receiving the luminal flow information from the Fluid Dynamics Module, the tissue was meshed to accurately capture the transmural flow and drug delivery map. ANSYS ICEM CFD (ANSYS, Inc., Canonsburg, PA, USA) was used to generate a computational grid consisting of tetrahedral elements specifically refining the cells near the struts and, at the vicinity of strut-tissue contact sites. A mesh dependence study was conducted for a preliminary, proof of concept case to estimate the right sizing to assure the independency of numerical results from the computational mesh. A coupled CFD and mass transfer model was applied to conduct the Steady-state blood flow and transient mass transfer analysis to determine the flow velocity inside the lumen and porous artery and drug distribution in the arterial wall. Free drug transport inside the lumen is governed by the advection-diffusion model [10], while additional reaction terms were added for the Drug transport inside the arterial wall to account for binding [11].

$$\frac{\partial C_w}{\partial t} + R_F\left(\overrightarrow{V_w} . \nabla C_w\right) = D_w . \Delta C_w - \frac{\partial b_1}{\partial t} - \frac{\partial b_2}{\partial t} \quad (1)$$

The dynamics of drug bounding to the extracellular matrix (ECM) and the specific receptors (SR) are modelled by:

$$\frac{\partial b_1}{\partial t} = k_{a1} C_w (B_{1max} - b_1) - k_{d1} b_1 \quad (2)$$

$$\frac{\partial b_2}{\partial t} = k_{a2} C_w (B_{2max} - b_2) - k_{d2} b_2 \quad (3)$$

Where C_W is the drug concentration within the tissue and D_w denotes the diffusivity of the drug inside the wall, b_1 and b_2 are the drug concentration bound to the Extracellular Matrix (ECM) and Specific Receptors (SR) respectively, and for the ECM- and SR-bound drug k_{a1} and k_{a2} are association factors, k_{d1} and k_{d2} are dissociation factors, and B_{1max} and B_{2max} are maximum biding capacity, respectively[12]. Multiplication of the advection term with retardation factor (R_F) was ignored as R_F is equal to one for drugs with molecular weights within the range of 32 to 10000 Da [13] (958.22 Da herein for Everolimus). Flow boundary conditions were adopted from the Fluid Dynamics Module for the luminal flow, assuming symmetry for tissue inlet/outlet, and adventitial pressure at the outer wall. Conservation of advective flux at the mural surface was automatically applied, having the luminal wall defined as an interface between the fluid and porous domain. A Dirichlet zero free drug concentration was assigned at the inlet and open boundary condition and flux conservation are assumed at the outlets and the mural interface, respectively. The drug-coated surface would receive the flux boundary condition dictated by the release kinetics model and the flux on the uncoated surfaces of stent are set to zero. In cases of full apposition and abluminal drug delivery, only the tissue domain was modelled to economize the computational costs. In such cases, pure sink of drug (both free and bound) was considered at mural and adventitial surfaces. The entire domain was initialized with zero concentration at the simulation start time.

The total concentration of drug, bound and unbound, exhibits a strong dependency to the release flux, local tissue thickness, and the design of the stent (Fig. 6). Receptor saturation in the tissue exhibited strong spatial and time dependencies (not shown here), originally confined to peristrut sites, and later extended across the entire wall thickness of stented tissue and persisting for the entire period of simulations.

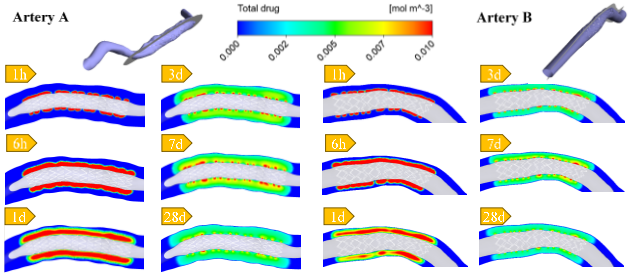

Figure 6: Total drug concentration at different time points for the patient A and patient B, with the insets where the 2D cross section has been made.

Total drug uptake kinetics were calculated as a volume-averaged summation of bound and unbound drug (Fig. 7). A pattern of considerable uptake at early stages of burst release is observed. For this stent, our results revealed that there is not significant sensitivity of drug uptake to lesion morphology and arterial geometry, with the current simulation setup. This is mainly due to high affinity receptor binding, which is seen to maintain a rather uniform distribution of drug, confirming robust performance in clinics for industry-level devices.

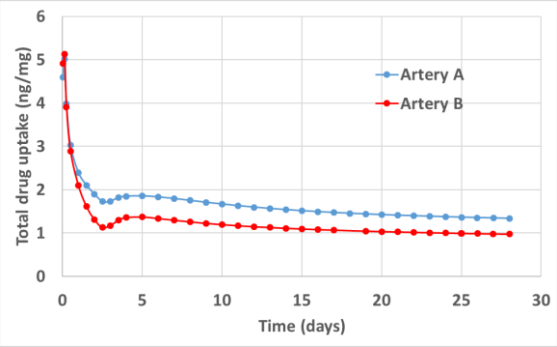

Figure 7. Calculated flux for the Synergy applied in the simulation.

III. Conclusion

This study presented a first attempt of demonstrating scenario II using patient-specific anatomies and a commercially available stent. The results indicate that the Synergy stent is able to reopen the lumen in both cases without risk of stent damage. In the Artery A, however, the vessel is subjected to high deformation that could potentially lead to restenosis. In addition, it was shown that the drug retention is not significant sensitive to lesion morphology due to high affinity receptor binding, which is able to maintain a rather uniform distribution of drug over the course of 30 days, confirming the robust performance in clinics for current devices.

Concluding, it has been demonstrated that computational modeling of stent implantation performance in patient-specific geometries allows the prediction of clinical endpoints and additional variables of interest that cannot be foreseen from real clinical trials, however to provide concrete conclusions, this paradigm should be applied in a larger number of patient specific cases and validated using data from an parallel clinical study.

References

[1] https://www.globenewswire.com/news-release/2020/09/16/2094355/0/en/Global-Medical-Device-Industry-Statistics-Show-Production-Of-Non-COVID-Equipment-Is-Severely-Impacted.html. .

[2] “Synergy - Everolimus-Eluting Platinum Chromium Coronary Stent System - Boston Scientific.” https://www.bostonscientific.com/en-EU/products/stents-coronary/synergy-stent-system.html (accessed Jan. 27, 2020).

[3] C. V. Bourantas et al., “A new methodology for accurate 3-dimensional coronary artery reconstruction using routine intravascular ultrasound and angiographic data: implications for widespread assessment of endothelial shear stress in humans,” EuroIntervention J. Eur. Collab. Work. Group Interv. Cardiol. Eur. Soc. Cardiol., vol. 9, no. 5, pp. 582–593, Sep. 2013, doi: 10.4244/EIJV9I5A94.

[4] J. E. Davies et al., “Evidence of a dominant backward-propagating ‘suction’ wave responsible for diastolic coronary filling in humans, attenuated in left ventricular hypertrophy,” Circulation, vol. 113, no. 14, pp. 1768–1778, Apr. 2006, doi: 10.1161/CIRCULATIONAHA.105.603050.

[5] A. G. van der Giessen et al., “The influence of boundary conditions on wall shear stress distribution in patients specific coronary trees,” J. Biomech., vol. 44, no. 6, pp. 1089–1095, Apr. 2011, doi: 10.1016/j.jbiomech.2011.01.036.

[6] Ansys Fluent, Release 20.1, Help System, Fluent User’s Guide, Chapter 7, section 7.4.11, ANSYS, Inc. .

[7] F. Gijsen et al., “Expert recommendations on the assessment of wall shear stress in human coronary arteries: existing methodologies, technical considerations, and clinical applications,” Eur. Heart J., vol. 40, no. 41, pp. 3421–3433, Nov. 2019, doi: 10.1093/eurheartj/ehz551.

[8] A. R. Tzafriri, F. R. Nezami, and E. R. Edelman, “CRT-500.06 Computational Prediction of Drug-Eluting Stent Performance in Patient-Specific Arteries: A Virtual Reality,” JACC Cardiovasc. Interv., vol. 13, no. 4, Supplement, pp. S43–S44, Feb. 2020, doi: 10.1016/j.jcin.2020.01.137.

[9] N. Benard, R. Perrault, and D. Coisne, “Computational approach to estimating the effects of blood properties on changes in intra-stent flow,” Ann. Biomed. Eng., vol. 34, no. 8, pp. 1259–1271, Aug. 2006, doi: 10.1007/s10439-006-9123-7.

[10] F. Rikhtegar, E. R. Edelman, U. Olgac, D. Poulikakos, and V. Kurtcuoglu, “Drug deposition in coronary arteries with overlapping drug-eluting stents,” J. Control. Release Off. J. Control. Release Soc., vol. 238, pp. 1–9, Sep. 2016, doi: 10.1016/j.jconrel.2016.07.023.

[11] A. R. Tzafriri, A. Groothuis, G. S. Price, and E. R. Edelman, “Stent elution rate determines drug deposition and receptor-mediated effects,” J. Control. Release Off. J. Control. Release Soc., vol. 161, no. 3, pp. 918–926, Aug. 2012, doi: 10.1016/j.jconrel.2012.05.039.

[12] A. R. Tzafriri, A. D. Levin, and E. R. Edelman, “Diffusion-limited binding explains binary dose response for local arterial and tumour drug delivery,” Cell Prolif., vol. 42, no. 3, pp. 348–363, Jun. 2009, doi: 10.1111/j.1365-2184.2009.00602.x.

[13] E. A. Swabb, J. Wei, and P. M. Gullino, “Diffusion and Convection in Normal and Neoplastic Tissues,” Cancer Res., vol. 34, no. 10, pp. 2814–2822, Oct. 1974.